

## AN OPTIMIZATION APPROACH TO MODELING SEA ICE DYNAMICS, PART 2: FINITE ICE STRENGTH EFFECTS\*

HELGA S. HUNTLEY<sup>†</sup> AND ESTEBAN G. TABAK<sup>‡</sup>

**Abstract.** The effects of a finite ice strength on a new model for sea ice dynamics, deriving the internal pressure field from a global optimization problem, rather than a local rheology, are examined. Building on the promising results from the one-dimensional Lagrangian model described previously, here we add one of the key properties of sea ice. In order to investigate the behavior of the model under ice yielding, the equations are cast in an Eulerian framework, now allowing for variable thickness. The model is first tested under conditions of infinite ice strength, to ensure that the numerics behave as desired. A finite ice strength is incorporated into the model as a second optimization step, minimizing the change in ice thickness necessary to satisfy the upper bound on the pressure, whereby ice strength is taken to be a linear function of thickness, following typical parameterizations in the literature. The theory is implemented numerically, and several test cases are discussed, which show good agreement with physically based expectations.

**Key words.** ice dynamics, rheology, fluid dynamics, ice yielding

**AMS subject classifications.** 76M30, 86A05

**DOI.** 10.1137/060668651

**1. Introduction.** Much progress has been made in the field of sea ice dynamics modeling over the last half a century, as models have evolved from using free drift to incorporating complex rheologies, derived from various physical considerations. Nonetheless, some salient features of the polar ice covers (as, for example, sea ice arches in the straits of the Canadian Arctic Archipelago) are still not being reproduced satisfactorily. With the ultimate goal of remedying this shortfall, we are developing a novel method for modeling the dynamics.

In Part 1 of this study [6], we introduced a new way to calculate the internal stress arising in converging sea ice; here we discuss how a finite ice strength can be incorporated into the model. The theory was developed in a Lagrangian frame of reference. This simplified the equations to a degree that it was possible to verify the numerical model results by comparing them to an analytic solution to a well-understood toy problem. Beginning with the analogy that coarse grained sea ice can be described as a semi-incompressible fluid (i.e., a fluid that is always allowed to diverge, but can converge only if the ice strength is insufficient to stop the motion), it was argued that the problem of finding the internal stress can be phrased as an optimization problem, where the pressure plays the role of a Lagrange multiplier.

In order to be able to carry out a relatively straightforward qualitative analysis of the results, we make (in both Parts 1 and 2) several simplifications to the full ice dynamics problem. Thus, thermodynamic effects are ignored. We also do not incorporate a thickness distribution. Thorndike et al. [11] and subsequent studies argued

---

\*Received by the editors December 20, 2004; accepted for publication (in revised form) August 30, 2006; published electronically February 15, 2007. This article derives from work done as part of the Ph.D. thesis of Helga Schaffrin Huntley, while partially supported by the NSF VIGRE program. <http://www.siam.org/journals/siap/67-2/66865.html>

<sup>†</sup>Department of Applied Mathematics, University of Washington, Box 352420, Seattle, WA 98195-2420 (helga@amath.washington.edu).

<sup>‡</sup>Department of Mathematics, Courant Institute of Mathematical Sciences, New York University, 251 Mercer St., New York, NY 10012 (tabak@cims.nyu.edu). This author's work was partially supported by grants from the NSF Division of Applied Mathematics.

well for the importance of and provided a method for tracking such a distribution. It is particularly relevant for thermodynamics, as the freezing and melting properties of thin ice and thick ice differ significantly. However, since ice strength is also a function of ice thickness, resolving subgridscale variations is desirable even in a purely dynamic model. Realizing the resulting limitations, we ignore these effects. Similarly, we do not employ a velocity distribution, but consider all velocities mass-averaged over a grid cell. As the work reported here is intended as a feasibility study, we also set all external forces equal to 0. (They are easily added back into the dynamics, as will be described below, but complicate the analysis of the results.) Finally, we restrict ourselves to one dimension, where only isotropic stress exists. How to handle shear stresses will be addressed in subsequent work. The assumption from Part 1 that is dropped here is that of constant ice thickness throughout the domain, in order to allow crushing of the ice.

The appealing simplicity of the equations derived in the Lagrangian framework in Part 1 resulted in part from the assumption of a constant ice thickness. Permitting the thickness to vary over the domain and especially for individual floes (or their grid-averaged equivalent) due to yielding negates the advantages of the formulation we used previously. Thus, following a quick review of the Lagrangian model in section 2, we will here return to an Eulerian point of view. The new theory is presented, and the corresponding numerical model, with variable ice thickness but still infinite ice strength, is compared to the Lagrangian one of Part 1 in sections 3 and 4. In section 5, then, ice strength is limited, and ice is allowed to yield. For the parameterization of ice strength, we rely on suggestions from the literature. (Note that, as we are not carrying out quantitative studies or direct checks against data, the *form* of the parameterization is more important than the exact empirical—or tuned—values used.) It turns out that employing the limiting ice strength as a truncation value for the internal pressure directly leads to undesirable effects. Hence, we instead reformulate the problem in terms of a double optimization, where the ice strength becomes a new constraint on the pressure. Some numerical results are discussed in section 6, and conclusions presented in section 7. The appendix provides some of the mathematical details of the model derivation; for greater detail on some of the other results, the reader is referred to [10].

**2. Lagrangian dynamics.** We will use the same notation as in Part 1 [6]. In particular, the variables are defined as follows:

- $c$  = concentration of ice (fraction of sea surface area covered by ice),
- $h$  = thickness of the ice, averaged over a grid box,
- $u$  = horizontal velocity,
- $F$  = sum of all forces under consideration,
- $p$  = internal stress.

Recall that we are not modeling any thermodynamic effects, so that all sources and sinks of ice (melting, freezing, and precipitation) are set to 0. Similarly, no forces other than the internal stress are considered in this paper, so that  $F$  denotes the force due to the internal stress. The density of ice, which is nearly constant, is taken to be identically 1. Alternatively, one can consider it as absorbed in  $h$ , which then represents the product of ice thickness and density or, in effect, an areal density. The authors find it most useful, however, to continue thinking of  $h$  as thickness.

The Eulerian spatial coordinate will be denoted by  $x$ , while the Lagrangian mass coordinate is given by

$$(1) \quad \xi = \int_0^x ch \, d\hat{x}.$$

For the Lagrangian formulation, we also define the new variable

$$k = \frac{1}{ch} - 1,$$

which simplifies the form of the governing equations.

The mass and momentum conservation equations in one dimension are given, in Eulerian coordinates, by

$$(2) \quad (ch)_t + (chu)_x = 0,$$

$$(3) \quad (chu)_t + (chu^2)_x = F.$$

We will return to these in the next section.

Translating the system into the Lagrangian coordinate defined above in (1) and substituting the new variable  $k$  yields

$$(4) \quad k_t = u_\xi,$$

$$(5) \quad u_t = \tilde{F},$$

where  $\tilde{F} = F/(ch)$  is still unknown.

We argued in Part 1 [6] (where ice strength was taken to be infinite) that the internal stress arises solely due to the semi-incompressibility of the ice. It serves the purpose of preventing further convergence when  $c = 1$ , or, in other words, of enforcing the constraint that  $c \leq 1$ , equivalently that  $k \geq 0$  (for  $h$  constant and taken to be 1). Consequently, it was suggested that the problem of finding  $F$  amounts to a constrained optimization problem, which can be solved using Lagrange multipliers. The pressure arose naturally as such a multiplier. It was shown that for the case without ice yielding, minimizing  $\|p\|$  is equivalent to minimizing  $\|p_\xi\|$ . So the system was ultimately phrased as follows:

$$(6) \quad \text{minimize } \|p\|,$$

$$(7) \quad \text{subject to the constraints } k_t = u_\xi,$$

$$(8) \quad u_t = -p_\xi,$$

$$(9) \quad k \geq 0,$$

$$(10) \quad p \geq 0.$$

As the numerical model arising from this theory behaved well under the verification tests (comparison to an analytic solution, comparison with a particle-resolving model, and qualitative assessment of other model runs), we concluded that this approach to sea ice dynamics is promising.

The analysis carried out in Part 1 [6], however, relied on the unrealistic assumptions of constant ice thickness and infinite ice strength. This paper is intended to carry the model one step further by eliminating those simplifications.

**3. Translation to Eulerian coordinates.** Allowing variable ice thickness in the Lagrangian model outlined in the previous section leads to some difficulties. For one, the constraint on  $k$  becomes the rather cumbersome  $k \geq \frac{1-h}{h}$ , versus the simple  $k \geq 0$ . In fact, this constraint is not even well defined if we let  $h = 0$ . Of course, in this case,  $c$  is also somewhat arbitrarily defined, but it is preferable to work with a variable that is not occasionally constrained to be greater than or equal to infinity. It should also be noted that the Lagrangian mass coordinate distorts the resolution in favor of thick ice. In the discretized optimization, then, minimizing the pressure in thicker parts weighs heavier than doing so for thinner parts, which distorts the pressure field as well. These observations argue strongly for proceeding in Eulerian coordinates. In addition, it is unclear whether the mass coordinates can be extended into a second dimension while retaining any of the desired simplifications. Thus, we return to Eulerian coordinates for studying the effects of a finite ice strength.

Translating the system (6)–(10) into Eulerian coordinates results in

$$\begin{aligned} (11) \quad & \text{minimize } \|p\|, \\ (12) \quad & \text{subject to the constraints } (ch)_t + (chu)_x = 0, \\ (13) \quad & (chu)_t + (chu^2)_x = -p_x, \\ (14) \quad & 0 \leq c \leq 1, \\ (15) \quad & 0 \leq p. \end{aligned}$$

As a side note, if one had decided not to ignore external forces, these could easily be added to the left-hand side of (13). Everything that follows could be carried out as described here (except, of course, that a discretization would have to be found for the additional terms).

The reader will notice that even once  $p$  is determined by the optimization, there are but two equations for the three unknowns  $c$ ,  $h$ , and  $u$ . Let us continue to assume infinite ice strength for now, before adding this additional complexity in the next section. In this case, since ice does not crush, it is reasonable to take ice thickness to be conserved following ice floes, or, in other words,  $h$  to be advected:

$$(16) \quad h_t + u h_x = 0.$$

Using the mass conservation equation (12), we can rewrite this as

$$(17) \quad c_t + (cu)_x = 0.$$

This equation is then added as an additional constraint to the optimization problem (11)–(15).

For the numerical implementation, we chose to rewrite the momentum conservation equation as a velocity evolution equation:

$$(18) \quad u_t + \left( \frac{u^2}{2} \right)_x = -\frac{p_x}{ch}.$$

Retaining momentum ( $chu$ ) as a fundamental variable to be updated each time step is attractive, since it can then be exactly conserved. However, a preliminary numerical implementation following this approach proved to be far more prone to numerical instabilities than one updating velocity explicitly. (It may be worth mentioning that velocity is updated directly in many of today's ice dynamics models; see, e.g., [4] and [5].)

Note that this derivation is valid only if  $c \neq 0$ . However, wherever  $c = 0$ , the velocity is intrinsically not well defined as a physical quantity. Defining the ratio on the right-hand side of (18) to be 0 in this case and evolving  $u$  accordingly provides for a solution for  $u$  to fill in the gaps. This particular choice has the advantage that regions without ice do not have to be treated separately in the numerical implementation. At first glance, one might expect that defining the ratio on the right-hand side to be 0 when  $c = 0$  might lead to strange discontinuities in the forcing, since  $\lim_{c \rightarrow 0} 1/c = \infty$ . Yet there is no inconsistency, since the pressure is also zero whenever  $c$  is far from 1. The situation with  $h = 0$  can be handled similarly. In this case, both  $u$  and  $c$  are arbitrary, so that  $c$  can be taken far from 1.

While advancing momentum as a fundamental variable leads to undesirable effects, we do retain mass ( $ch$ ) as a fundamental variable, so that it can be conserved exactly. Thickness  $h$  never appears explicitly in the equations. It is tracked as a derived variable.

A staggered grid is used, defining  $u$  at half steps from  $c$ ,  $ch$ , and  $p$ . This follows the setup for the Lagrangian model. Unlike in that case, however, it is here unfortunately not possible to avoid all need for interpolation of any variables. The placement of the variables was chosen to allow for a semi-implicit discretization for (17) (necessary to be able to satisfy the constraint on  $c$ ) and to keep mass and concentration in the same locations for deriving thickness.

The discretizations of (17), (12), and (13) take the form

$$(19) \quad c_{j+\frac{1}{2}}^{n+1} = c_{j+\frac{1}{2}}^n - \frac{\Delta t}{\Delta x} (c_{j+1}^n u_{j+1}^{n+1} - c_j^n u_j^{n+1}),$$

$$(20) \quad (ch)_{j+\frac{1}{2}}^{n+1} = (ch)_{j+\frac{1}{2}}^n - \frac{\Delta t}{\Delta x} ((ch)_{j+1}^n u_{j+1}^{n+1} - (ch)_j^n u_j^{n+1}),$$

$$(21) \quad u_j^{n+1} = u_j^n - \frac{1}{2} \frac{\Delta t}{\Delta x} \left[ \left( u_{j+\frac{1}{2}}^n \right)^2 - \left( u_{j-\frac{1}{2}}^n \right)^2 \right] - \frac{\Delta t}{\Delta x} \frac{1}{(ch)_j^n} \left[ p_{j+\frac{1}{2}}^{n+1} - p_{j-\frac{1}{2}}^{n+1} \right].$$

Observe that (20) serves only to update the variable ( $ch$ ); it does, in fact, not represent an additional constraint in the optimization. Thus, the linear constraint for the minimization of  $\|p\| = \sum p_i$  is given by (19), where (21) is used to substitute for  $u^{n+1}$ . The optimization provides updated values of  $p$  and  $c$ , which are then used to find updated values of  $u$  and subsequently of ( $ch$ ). The variables are interpolated where necessary by a Godunov-type scheme. (See the appendix for more details.) The results presented here were obtained from an implementation on Matlab, using the built-in “`linprog`” function for the minimization, which uses a linear interior point solver. (Alternatively, a simplex method can be prescribed. The resulting differences in the output are negligible.) Also, periodic boundary conditions were imposed.

**4. Results in Eulerian coordinates without yielding.** A series of tests was carried out on this model to check its behavior under various initial conditions. Here we will present only two of the results. First, we will compare the behavior of this Eulerian model to that of the Lagrangian one from Part 1 [6]. The equations and hence the numerics are more complicated here, requiring the choice of an interpolation scheme in addition to a discretization. Moreover, it can be shown that, with the choices made here, in general,

$$\sum_j (ch)_j^{n+1} u_j^{n+1} - \sum_j (ch)_j^n u_j^n \neq 0.$$

In other words, momentum is not exactly conserved. It is, thus, desirable to check that the deviations are acceptably small.

For the comparison, we initialize both models with a sinusoidal initial velocity, constant ice thickness ( $h_o = 1$ ), and uniform ice concentration. Since spatial and temporal resolutions are fixed throughout the runs but space is measured in different coordinates, it is not possible to retain equivalent spatial step sizes in the two models. In particular, the specifications are as follows:

$$\begin{array}{ll} c_o = 0.5, & k_o = 1, \\ u_o = \sin(2\pi x), & u_o = \sin(4\pi\xi), \\ \Delta x = 0.0125, & \Delta\xi = 0.0125, \\ \frac{\Delta t}{\Delta x} = 0.1, & \frac{\Delta t}{\Delta\xi} = 0.1. \end{array}$$

(Recall that  $k$  was defined as  $k = (1 - ch)/ch$  and  $\xi = \int_0^x ch \, d\tilde{x}$ .)

For the plots, we have chosen four times:

$$\begin{array}{ll} t = 0.0175 & \text{fairly early on, after 15 time steps,} \\ t = 0.0500 & \text{shortly before consolidation begins, after 41 time steps,} \\ t = 0.0900 & \text{shortly after consolidation begins, after 73 time steps,} \\ t = 0.1500 & \text{about 2/3 through this run, after 121 time steps.} \end{array}$$

At each of these times, we have converted the Lagrangian spatial coordinate to the Eulerian one for a direct comparison. Figures 1 and 2 display the concentrations and velocities from the two models corresponding to these times. Figure 3 shows the momenta.

The two models show good agreement in both concentration and velocity; the lines coincide almost exactly. The differences are mostly due to resolution, as different points are resolved in each model. The same is true for the momentum plots. Here the Eulerian model produces somewhat greater values for both the positive and the negative velocities near the consolidated region, which may be related to the interpolation. (The momentum is the product of two quantities that are tracked in different spatial locations. Thus, even for the Lagrangian results, interpolation is necessary to calculate it.) Recall that the Lagrangian model was designed to conserve momentum exactly. The discretization chosen for the Eulerian model, on the other hand, does not do the same. (Of course, in the limit as the resolution becomes finer, this error vanishes.) The fact that the momentum profiles from the Eulerian model agree so well is evidence that momentum is close to being conserved here as well. Further support comes from the fact that the constant velocity at which the consolidated ice travels is 0 (up to four decimal places), just as predicted by the theory based on momentum conservation. (This velocity test, by the way, holds up in other examples as well, although the accuracy degrades somewhat to only  $10^{-2}$  when the average velocity is not 0. Some of this loss in accuracy can be ascribed to numerical diffusion.)

Before the ice begins to consolidate, the numerical solutions can also be compared to exact analytic solutions. Both the Lagrangian and the Eulerian model produce very good approximations (not shown). For the latter, the type of interpolation chosen can make a noticeable difference. (Again, see the appendix for a description of the scheme we use.) The first accumulation time (when  $c$  first reaches 1 and  $p$  becomes nonzero) is theoretically predicted in this example to be  $1/4\pi \approx 0.079577$ . The model here predicts it to be in the interval  $[0.07875, 0.08000]$ ; i.e., it captures it very well.

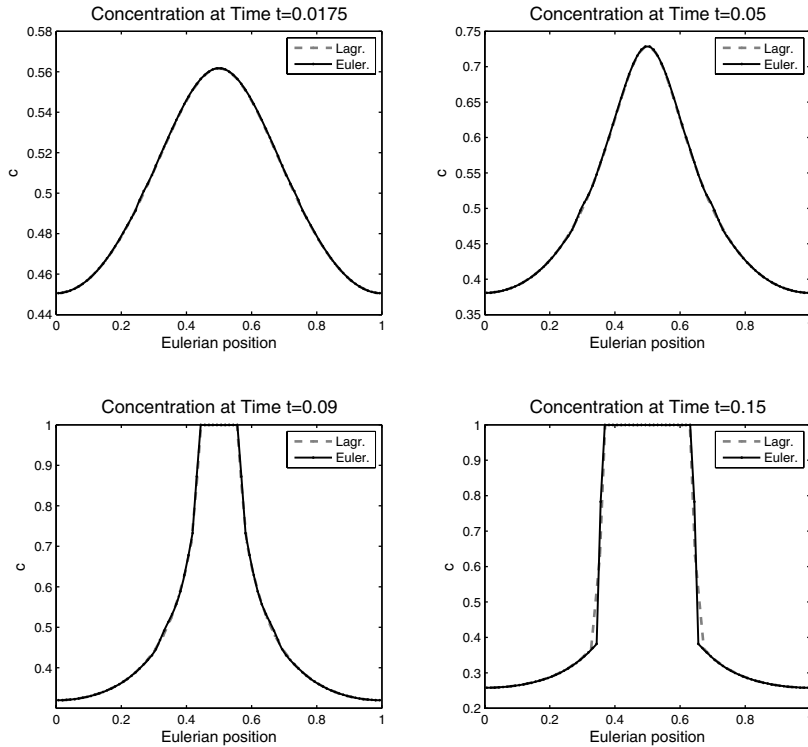


FIG. 1. Comparing ice concentrations at various times from the Lagrangian and the Eulerian models. The Eulerian output is interpolated with a solid black line, the Lagrangian with a dashed grey line.

To test how the model handles variable thickness (which, after all, was the primary purpose for it), we ran an example with a parabolic initial thickness distribution, while using again the sinusoidal initial velocity and uniform initial concentration. Figure 4 beautifully exhibits the behavior. As the ice is pushed together in the center of the domain, the thickness profile steepens. Once concentration reaches 1,  $h$  no longer changes. This agrees well with expectations from physical intuition.

**5. Incorporating finite ice strength.** Now that we have a model allowing for variable ice thickness, we can introduce the process of ice yielding.<sup>1</sup> It is well known that sea ice has a finite strength, which depends on ice thickness. It may also depend on other properties, such as the age of the ice or the salinity of the water from which it was formed. These variables are not being tracked in this model. The literature, moreover, seems to agree generally that thickness is the most important factor.

<sup>1</sup>We will use the terms “yielding,” “crushing,” and “ridging” interchangeably, although the actual processes of crushing and ridging may be quite different. Ridging typically occurs when ice floes slide under each other, while crushing implies that the ice actually breaks. The net result of both processes is thicker ice, as a consequence of yielding. It is generally accepted that resistance to crushing is significantly higher than that to ridging. Hence, most of the yielding accounted for here will technically be ridging rather than crushing.

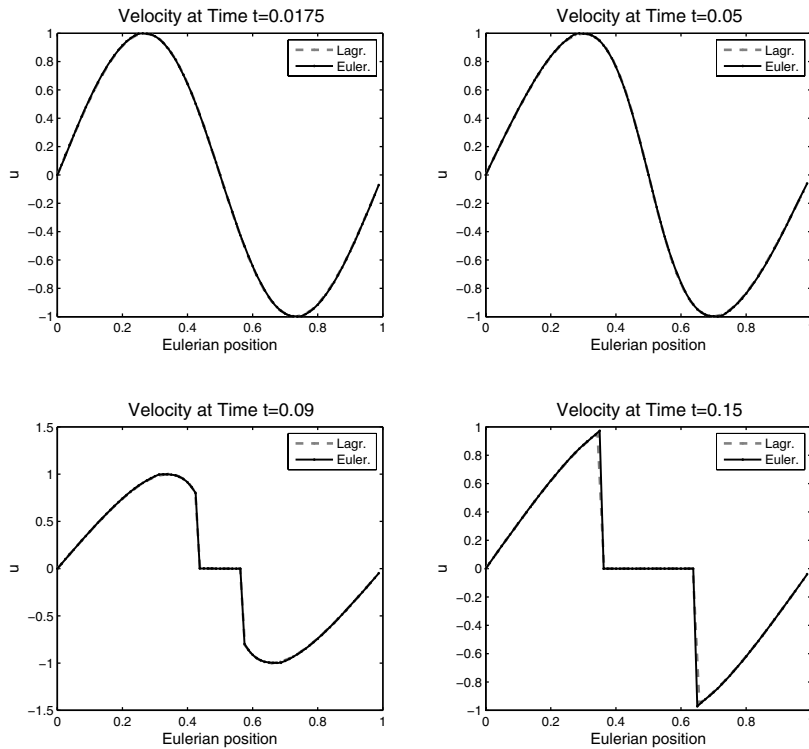


FIG. 2. Comparing ice velocities at various times from the Lagrangian and the Eulerian models. The Eulerian output is interpolated with a solid black line, the Lagrangian with a dashed grey line.

Ice dynamics models currently in use do not typically include dependence on anything but ice thickness and concentration.

The importance of a failure criterion for sea ice dynamics has been recognized at least since the mid-1970s (see [1]). It has been incorporated into plastic (e.g., [8]), viscous-plastic (e.g., [4]), elastic-plastic (e.g., [2] and [9]) and elastic-viscous-plastic (e.g., [5]) rheologies, but it has also appeared in other descriptions of the constituency law for ice, such as the cavitating fluid (e.g., [3]) and granular flow (e.g., [12]) rheologies.

The literature offers essentially two types of ice strength parameterizations. On the one hand is a formulation relating ice strength  $P^*$  to the potential energy change associated with the changes in ice thickness. This was first suggested by [9], was adopted by [11], and has been used ever since in connection with the thickness distribution theory pioneered by the latter.

For simpler models, using a two-category thickness distribution, distinguishing within a grid box only between ice and open water (the type employed here), ice strength has uniformly been taken as a function of ice thickness and concentration, although the functional dependence is not always the same. The other factors that may influence ice strength (such as age) are generally not taken into account.

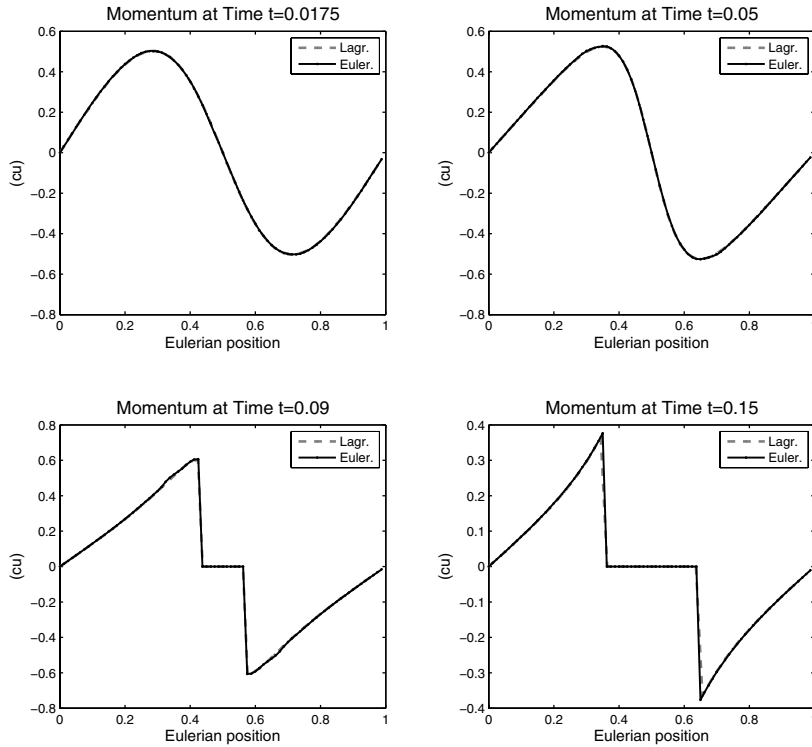


FIG. 3. Comparing ice momenta at various times from the Lagrangian and the Eulerian models. The Eulerian output is interpolated with a solid black line, the Lagrangian with a dashed grey line.

Most models follow the formulation presented by [4]:

$$(22) \quad P^* = P_o c h e^{-b(1-c)},$$

where  $P^*$  is the ice strength expressed as a maximal pressure and  $P_o$  and  $b$  are empirical parameters.<sup>2</sup> This parameterization exhibits several of the desired properties. The thicker the ice, the stronger it is. The greater the concentration, the greater is the total strength. However, it is also apparent that even if  $c$  is relatively far from 1 (say 0.6 or so), the ice strength is still significant.

Overland and Pease [8] suggest an alternative. Instead of a linear dependence on  $h$ , a quadratic law is hypothesized, which leads to a better approximation in their study of observed ridging:

$$(23) \quad P^* = P_o \rho c h^2 e^{-b(1-c)}.$$

The only other difference is that they include a dependence on ice density, which is typically (as in this work) taken to be a constant and can hence be absorbed into  $P_o$ . The functional form (22) has proven to be the more popular of these two.

<sup>2</sup>Hibler's notation in the 1979 paper [4] is actually  $P = P^* h \exp[-C(1-A)]$ . The formulation here reflects the definition of the variables we are using throughout. Note also that Hibler's  $h$  is an *effective* ice thickness, i.e., more akin to  $ch$  in our notation.

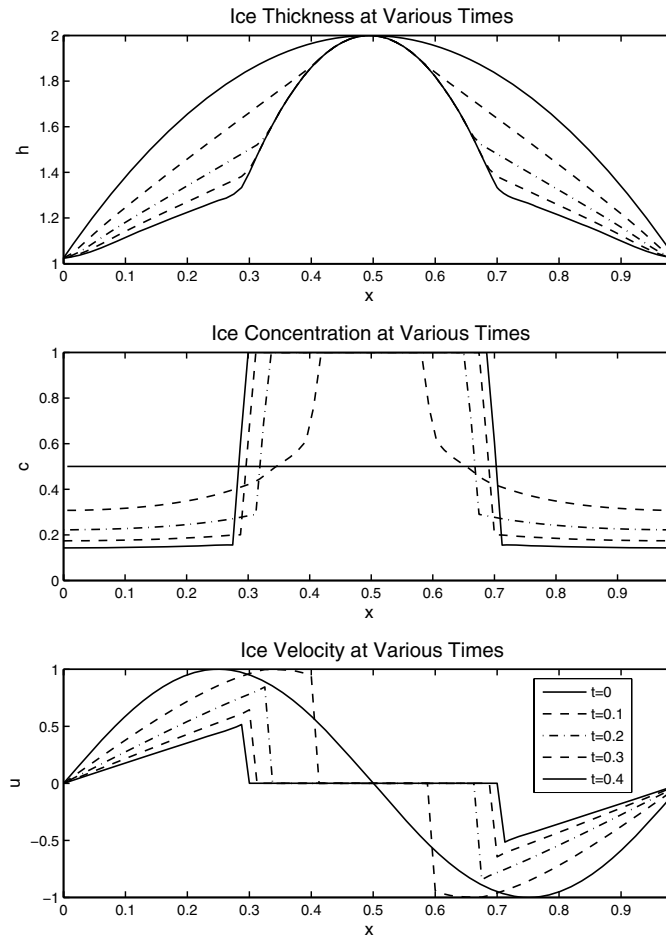


FIG. 4. The Eulerian model was run with spatial step size set to 0.0125 and temporal step size set to 0.00125. Initial conditions were  $c_o = 0.5$ ,  $h_o = -4x^2 + 4x + 1$ , and  $u_o = \sin(2\pi x)$ . The evolution of  $h$ ,  $c$ , and  $u$  is illustrated in parallel with snapshots from five different times.

For our purposes, either description would work; we have chosen a linear dependence of ice strength on ice thickness, mirroring (22). However, we do not include the dependence on ice concentration. One of the underlying assumptions of our model is that  $p = 0$  whenever  $c \neq 1$ . Hence ice strength is irrelevant (or could be taken to be 0: the ice does not resist convergence) in this situation. Setting  $c = 1$  in (22), the parameterization becomes simply

$$(24) \quad P^* = P_o h.$$

Flato and Hibler found empirical values for  $P_o$  (and the  $b$  appearing in the exponential term of (22)) in their 1992 paper [3]. We are not, at present, concerned with

producing *quantitatively* correct results and will hence adjust  $P_o$  to assist in investigating the effect of a limiting pressure value, rather than using their recommendation or an otherwise physically justified value.

Initially, the limiting ice strength was treated as a truncation value for the pressure.  $p$  was calculated as before as the solution to the constrained minimization problem (11) with constraints (13)–(15) and (17). Then it was truncated by  $P^*$ . The resulting values for  $p$  were used to calculate the updated values for  $u$  and  $(ch)$  using (14) and (12). Equation (17) no longer holds where ice begins to yield. Thus, it is valid only in regions without crushing. However, since ice only yields where it is consolidated, we know that everywhere else  $c = 1$ .

This procedure is not advisable. Since the limiting values of  $p$  depend on  $h$ , the truncated  $p$  can have undesirable shapes. In particular, a convex thickness can lead to a convex pressure, which causes the ice to diverge artificially. The error in this procedure lies in the assumption that ice yielding in one area of a consolidated region does not change the pressure anywhere else. This, however, is not necessarily true.

The algorithm we would like to suggest here hence rephrases the optimization problem, instead of attempting to correct the pressure profile after the minimization. The finite ice strength is, in fact, an additional constraint for the optimization. On the other hand, we lose the constraint (17), since we can no longer assume advection of thickness. This poses problems, since we need to be able to say something about the advanced  $c$ , in order to constrain it to stay between 0 and 1.

Observe that as long as the ice is not allowed to yield,  $\frac{Dh}{Dt} = h_t + u h_x = 0$ ; ice thickness does not change following particles. When ice does buckle, it does so only to the degree necessary to satisfy the upper bound on the internal pressure. One can argue that  $h$  will change as little as possible—suggesting a second constrained optimization.

The new procedure then is as follows:

- (1) Minimize the changes in ice thickness globally:

$$(25) \quad \text{find} \quad \min \left\| \frac{Dh}{Dt} \right\|,$$

$$(26) \quad \text{given the constraints} \quad (ch)_t + (chu)_x = 0,$$

$$(27) \quad (chu)_t + (chu^2)_x = -p_x,$$

$$(28) \quad \frac{Dh}{Dt} \geq 0,$$

$$(29) \quad 0 \leq c \leq 1,$$

$$(30) \quad 0 \leq p \leq P^*.$$

The first inequality constraint (28) arises because crushing can only increase ice thickness. Equation (26) again is used to advance  $(ch)$  rather than as a true constraint on the problem. The norm for (25) is chosen to be the 1-norm, primarily for numerical considerations: This choice keeps the problem linear.

This minimization will give values for  $c$  and  $p$ , which determine  $u$  and  $h$ , at the new time level that minimize  $\left\| \frac{Dh}{Dt} \right\|$ . However, the answer is typically not unique. The only unique quantity is the  $\min \left\| \frac{Dh}{Dt} \right\|$ .

- (2) The first step provides the closure for  $h$ , so that it is now possible to proceed

with the pressure minimization:

$$(31) \quad \text{find } \min \|p\|,$$

$$(32) \quad \text{given the constraints } (ch)_t + (chu)_x = 0,$$

$$(33) \quad (chu)_t + (chu^2)_x = -p_x,$$

$$(34) \quad \left\| \frac{Dh}{Dt} \right\| = \text{value found in step (1)},$$

$$(35) \quad \frac{Dh}{Dt} \geq 0,$$

$$(36) \quad 0 \leq c \leq 1,$$

$$(37) \quad 0 \leq p \leq P^*.$$

Note that the first inequality (35) needs to be retained in addition to the last equality constraint (34), since it is a pointwise, rather than an integral, statement.

This minimization must have a solution for  $c$  and  $p$ , from which  $u$  and  $h$  are derived, satisfying all the constraints, since one was found in the first step.

In the case where no ice yielding occurs, this two-step algorithm simplifies to the procedure outlined in section 3 above, as desired: The minimum of  $\|Dh/Dt\|$  is zero. Since  $Dh/Dt$  is constrained to be nonnegative pointwise, this implies that, in fact,  $Dh/Dt = 0$  everywhere. This is the constraint used in section 3.

The numerical implementation follows the pattern above, for the model without ice yielding. The same grid and discretizations are used. Recall that the variable  $h$  is not directly updated at each time step. The objective function for the first minimization is hence rewritten in terms of  $(ch)$  and  $c$ . It follows from mass conservation (see (26)) that

$$(38) \quad c[h_t + uh_x] = -h[c_t + (cu)_x].$$

Since  $c \geq 0$  and  $h \geq 0$ , the inequality constraint  $\frac{Dh}{Dt} \geq 0$  is equivalent to  $c_t + (cu)_x \leq 0$ . Also, ice only crushes where  $c = 1$ . In other words, if  $c \neq 1$ , then  $\frac{Dh}{Dt} = 0$ . Hence minimizing  $\left\| \frac{Dh}{Dt} \right\|$  is equivalent to minimizing  $\left\| c \frac{Dh}{Dt} \right\|$  or  $\left\| -\frac{(ch)}{c} [c_t + (cu)_x] \right\|$ .

**6. Results with ice yielding.** To illustrate the effects of finite ice strength, we present here the model results from two different problems. First, we look at a somewhat degenerate example, where the initial ice thickness is taken to be constant. (Of course, here it does not remain constant, since  $P_o$  is chosen so that the ice does yield.) The initial concentration is also set constant at 0.5, while the velocity is initialized with a sine-curve.

Figure 5 shows the evolution of  $h$ ,  $c$ , and  $u$  during the run up to time  $t = 0.2$ . As expected, the ice begins to consolidate in the center of the domain. Shortly after the concentration reaches 1, the pressure begins to exceed the ice strength, and the ice begins to ridge. Initially, this happens right at  $x = 0.5$ . Later, the ice yields at the edges of the consolidated region, where it is still thinner (not having ridged there yet), leading to a profile with multiple peaks. This can be seen in Figure 6, which shows several snapshots of the ice thickness from this run.

The attentive reader may have noticed a slight inconsistency in Figure 6: At some times (e.g.,  $t = 0.08750$  or  $t = 0.10500$ ) the ice thickness actually decreases below its initial value of  $h = 1$ . This should not happen. On the other hand, these deviations

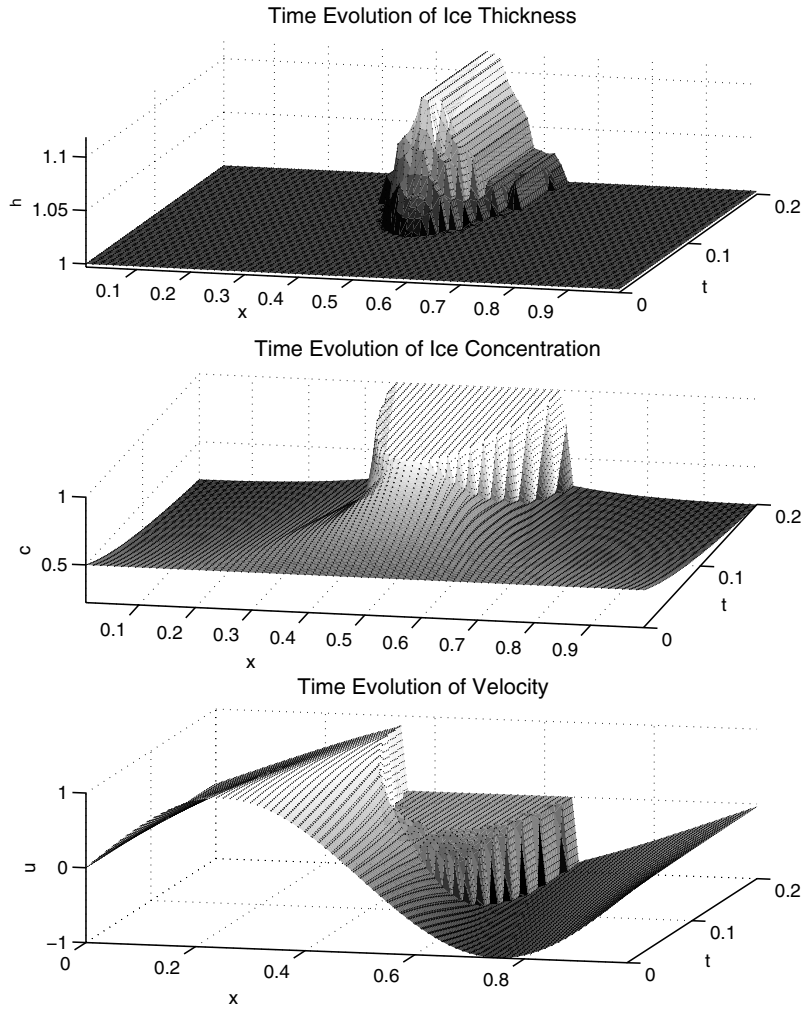


FIG. 5. The model allowing for crushing was run with spatial step size set to 0.0125 and temporal step size set to 0.00125. Initial conditions were  $c_o = 0.5$ ,  $h_o = 1$ , and  $u_o = \sin(2\pi x)$ .  $P_o$  was set to 2. The evolution of  $h$ ,  $c$ , and  $u$  is shown up to time  $t = 0.2$ .

are on a small scale, i.e., never greater than about 0.003. Moreover, recall that  $h$  is a derived quantity. The locations of the too-small values for  $h$  are invariably at the very edge of the consolidated domain, so that it stands to reason that the errors are due to a not quite precise enough capturing of the discontinuity in  $c$ . Indeed a higher spatial resolution does improve the situation. Thus, a halving of  $\Delta x$  leads to a reduction of the dips in  $h$  below 1 by a whole order of magnitude.

As a second example, we will examine a case where the ice thickness is not uniform, so that it is easier to predict where the ice should yield first. The initial conditions for this run are  $c_o = 0.5$ ,  $h_o = \cos(2\pi x) + 1.1$ , and  $u_o = \sin(2\pi x) + 1.5$ . As expected,

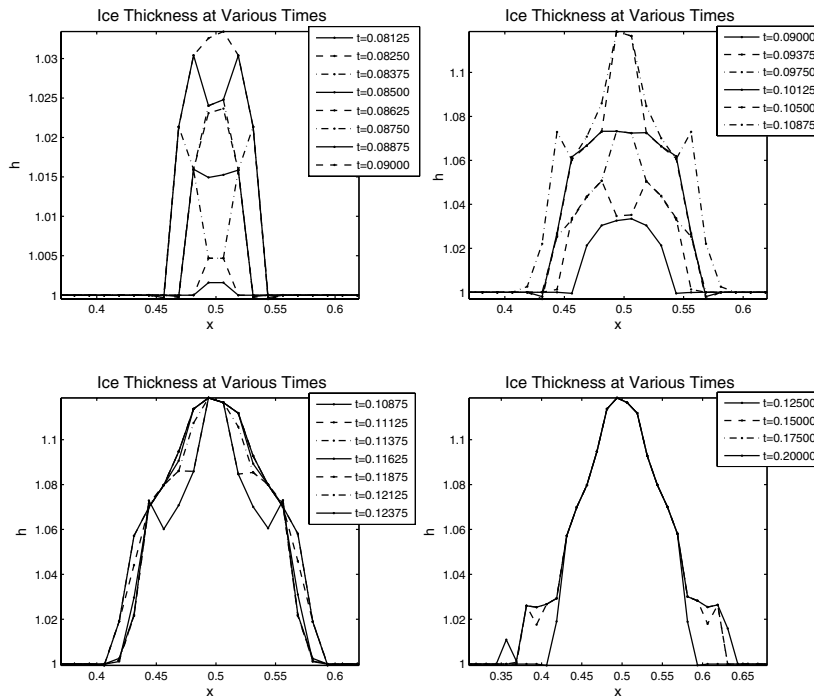


FIG. 6. Snapshots from the thickness evolution of the run from Figure 5. The ice yields initially at the center of the domain, but later at other points within the consolidated region, leading temporarily to profiles with multiple peaks.

the ice yields first where it is thinnest within the consolidated region. Figures 7 and 8 show the evolution of thickness, concentration, and velocity for this particular experiment. Note that the second figure is translated to the left, so that the center of the plot is at  $x = 1$  rather than at  $x = 0.5$ . (Recall that periodic boundary conditions are being used.)

For a more detailed look, Figure 9 shows  $h$ ,  $c$ , and  $u$  in one frame at two distinct times. In the plot on the left, for time  $t = 0.2$ , one can clearly see that the ice has begun to ridge in the consolidated region. It is also apparent that the velocity for this area is no longer constant; the yielding implies further convergence of the ice despite  $c$  equaling 1. In the plot on the right, for time  $t = 0.4$ , the ice is no longer yielding, and the consolidated ice travels at a uniform velocity of approximately 1.48 (close to the expected 1.5). By this time, the thickness profile within the region of  $c = 1$  is again a more or less smooth valley; the thinner parts from the earlier picture have ridged as well.

**7. Conclusions.** We are investigating the feasibility of a novel formulation of the sea ice dynamics. In Part 1 [6], the method for calculating the internal pressure term as the solution to an optimization problem was derived, and results of a Lagrangian model with infinite ice strength were discussed. In this part, we set out to show how a finite ice strength can be handled by a model of this type. The implementation turns out to be easier in an Eulerian framework. Thus, we translated the formulation,

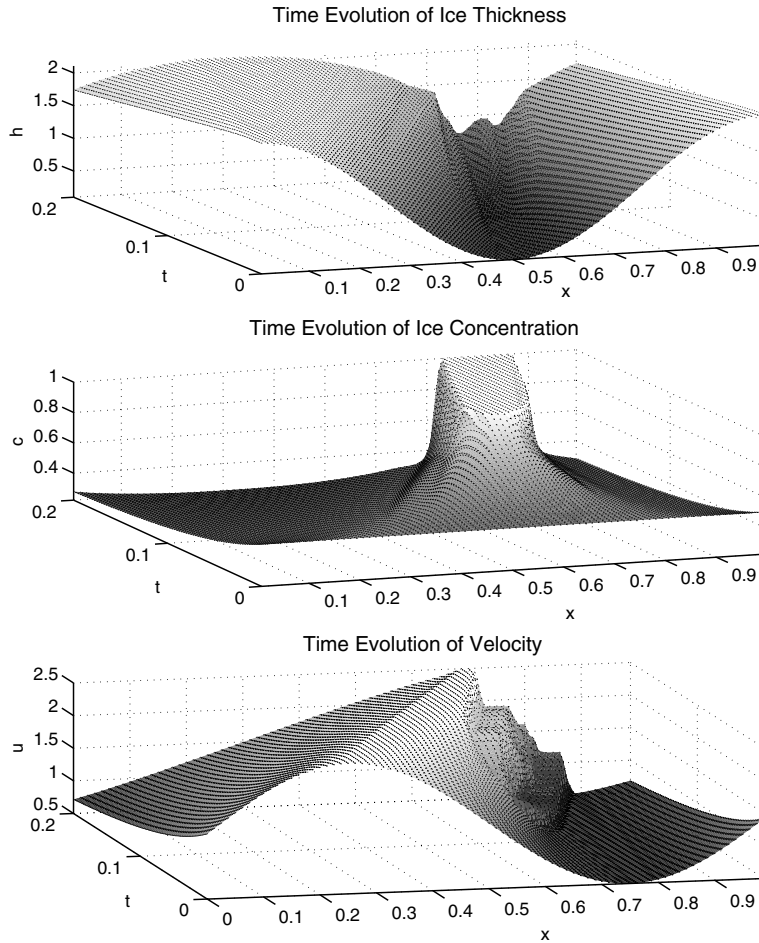


FIG. 7. The model allowing for crushing was run with spatial step size set to 0.0125 and temporal step size set to 0.00125. Initial conditions were  $c_o = 0.5$ ,  $h_o = \cos(2\pi x) + 1.1$ , and  $u_o = \sin(2\pi x) + 1.5$ .  $P_o$  was set to 1. The evolution up to time  $t = 0.2$  is shown. The ice begins to yield at the weakest point.

allowing now for a variable ice thickness, although initially still working with an infinite ice strength. This new model was compared to the Lagrangian one, to ensure that the choices made for the numerics, such as which variables to update explicitly at each time step and how to discretize the equations, did not lead to unreasonable results. In particular, we wanted to make sure that momentum, while not exactly conserved by the discretized equations, does not vary significantly over the course of a run. The Eulerian model output was also tested against an exact solution before consolidation, with very good agreement.

To incorporate a finite ice strength, we chose to adopt a parameterization of the ice strength as a multiple of the ice thickness, based on parameterizations common in the ice dynamics literature. Limiting the pressure the ice can withstand then requires

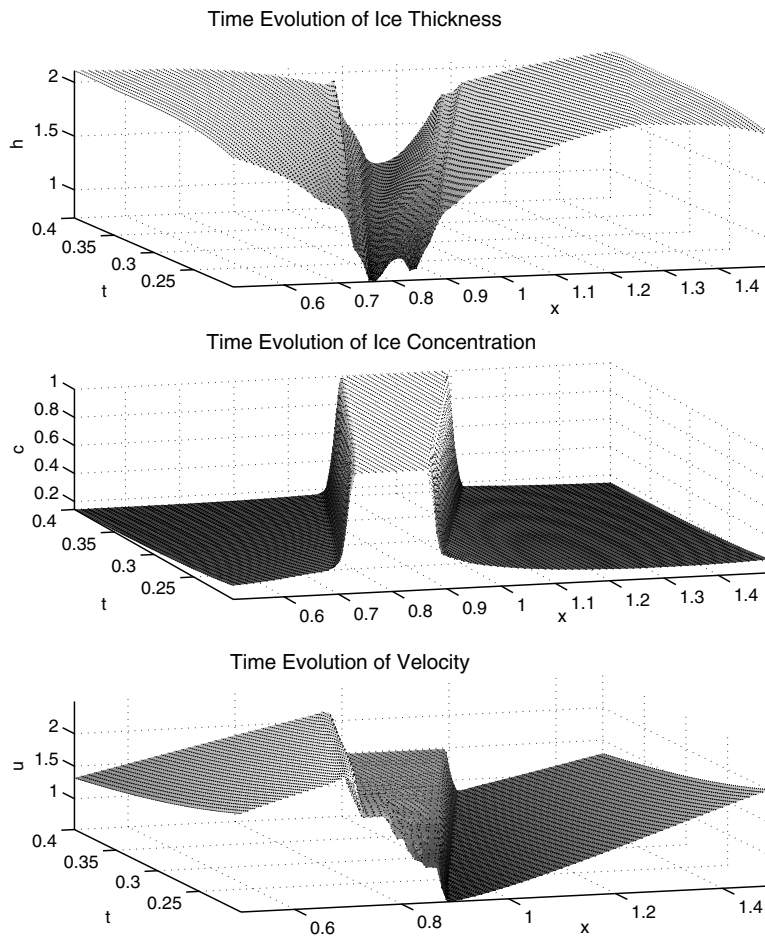


FIG. 8. The continuation of the plot in Figure 7; here the evolution from time  $t = 0.2$  until  $t = 0.4$  is shown. Thinner ice yields first, leading to a smooth convex profile for  $h$  within the consolidated region at the end of the run.

a second optimization problem, which determines how much the ice has to yield in order to satisfy this new constraint. While the solution to this minimization tends not to be unique, the minimum found is; this minimum then becomes an additional constraint on the second optimization, minimizing the pressure.

Two example runs were shown from this model, one beginning with a constant ice thickness, the second beginning with a varied one. In both cases, the behavior of the numerical results was qualitatively correct. Ice yields in the consolidated regions, whereby thinner ice tends to yield before thicker ice. Some convergence of the ice occurs during the ridging, but when the ice is thick enough to withstand the pressure exerted by the surrounding ice, all convergence is stopped—as desired.

It can be concluded, thus, that this procedure for determining internal stress for

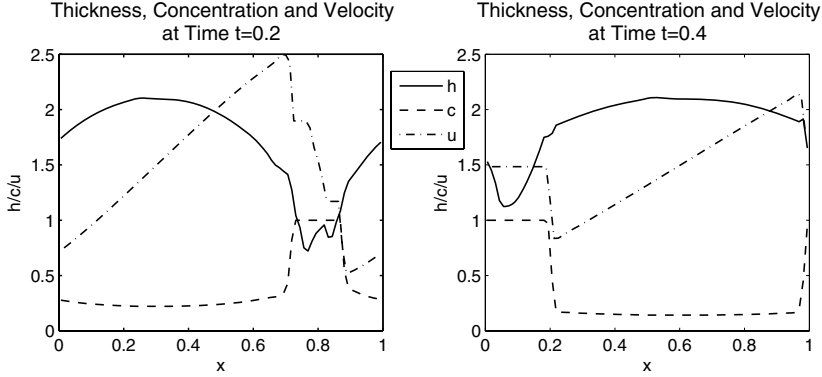


FIG. 9. Detail for the second experiment, as in Figures 7 and 8. The left panel shows thickness (solid line), concentration (dashed line), and velocity (dot-dashed line) at time  $t = 0.2$ . The right panel shows the same measures at time  $t = 0.4$ .

sea ice is indeed able to handle finite ice strength. Further work on a two-dimensional implementation is underway, where the new challenge of shear stresses and a limited shear strength arises. The findings presented here indicate that the method being investigated produces realistic results in one-dimensional cases, which is prerequisite to creating a working two-dimensional model.

**Appendix. Interpolation scheme.** As mentioned above, unlike the Lagrangian model, the Eulerian one requires that the variables be interpolated. They are defined on a staggered grid, but for the flux-form of the discretized equations we need to know their values at points in between. The strategy adopted here is a Godunov-type upwinding. See [7] for an extensive discussion of Godunov schemes.

For the concentration  $c$  and mass ( $ch$ ), the upwinding works as follows:  $u$  is defined at the interfaces to which each of these is to be interpolated. The sign of the velocity determines the side from which the values are taken. In our implementation, we also perform a linear extrapolation. Thus, since  $c$  is defined at half steps of the grid,

$$(39) \quad c_j = \begin{cases} \frac{3}{2}c_{j-\frac{1}{2}} - \frac{1}{2}c_{j-\frac{3}{2}} & \text{if } u_j \geq 0, \\ \frac{3}{2}c_{j+\frac{1}{2}} - \frac{1}{2}c_{j+\frac{3}{2}} & \text{if } u_j < 0. \end{cases}$$

This method generally produces a better estimate of the value at the interface than a constant approximation (i.e., letting  $c_j$  equal either  $c_{j-\frac{1}{2}}$  or  $c_{j+\frac{1}{2}}$ ). However, one needs to include a safeguard not to overshoot the desired values. Thus, the extrapolations are capped by the minimum and the maximum of the adjoining points. If, for example, the extrapolation predicts a value for  $c_j$  larger than  $\max\{c_{j-\frac{1}{2}}, c_{j+\frac{1}{2}}\}$ , then it is reset to the maximum (similarly for the minimum). The variable ( $ch$ ) is interpolated according to the same rules.

To find the value of  $u_{j+\frac{1}{2}}$  is a somewhat more complex problem. One wants to solve the local Riemann problem for the system of equations

$$(40) \quad c_t + (ch)_x = 0,$$

$$(41) \quad (ch)_t + (chu)_x = 0,$$

$$(42) \quad (chu)_t + (chu^2)_x = -p_x.$$

(We assume no crushing here in between two time steps.) It turns out, however,

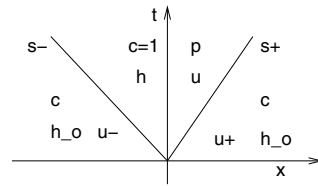


FIG. 10. *The two-shock setup with  $c^- = c^+$  and  $h^- = h^+ = h_o$ .*

that this system of equations has only one set of characteristics and only one Riemann invariant. This is insufficient in general. In the case of divergence or contact discontinuities, there is no convergence, and hence we can assume that  $p = 0$  is a solution. This observation allows us to simplify the momentum equation (42), using mass conservation (41), to Burgers' equation

$$(43) \quad u_t + \left( \frac{u^2}{2} \right)_x = 0.$$

Classical theory provides a solution to the local Riemann problem here. Thus, if we denote by  $u^-$  and  $u^+$  the extrapolated values to the left and to the right, respectively, of the interface, then

$$(44) \quad u_{j+\frac{1}{2}} = \begin{cases} u^- & \text{if } u^+ \geq u^- \geq 0, \\ u^+ & \text{if } u^- \leq u^+ \leq 0, \\ 0 & \text{if } u^- < 0 < u^+. \end{cases}$$

The case of convergence and shocks is a little trickier. In fact, it can be shown that now  $p$  cannot be 0. Physical considerations suggest that when ice converges, not one but two discontinuities in the velocity form, one on each side of the newly consolidated ice. The general case for a nonstaggered grid, where concentration, thickness, and velocity all differ from one side of the interface to the other, requires an additional assumption, such as pressure minimization or thickness advection. (See [10] for a detailed discussion of this case.) Luckily, on the staggered grid we have chosen, this is not necessary. The two-shock setup of the local Riemann problem is illustrated in Figure 10. Ice thickness and concentration on each side of the interface (or the shocks, once these develop) are denoted by  $h_o$  and  $c$ , respectively. The velocities to the left and to the right (the extrapolated values) are denoted by  $u^-$  and  $u^+$ , as before. In between the shocks, the ice is consolidated; hence  $c = 1$ , the thickness is  $h$ , pressure  $p$ , and velocity  $u$ .

In the following derivation, we will assume that  $0 < c < 1$ ; the other cases will be treated separately below.<sup>3</sup> For each shock, there are three jump conditions derived from (40)–(42):

$$(45) \quad s = \frac{[cu]}{[c]} = \frac{[chu]}{[ch]} = \frac{[chu^2 + p]}{[chu]},$$

where  $s$  is the shock speed. Using  $s^-$  for the shock speed on the left and  $s^+$  for that

<sup>3</sup>This restriction is desirable to ensure that the denominators in the jump conditions are nonzero.

on the right, these six equations become

$$(46) \quad s^- = \frac{cu^- - u}{c - 1},$$

$$(47) \quad \frac{cu^- - u}{c - 1} = \frac{ch_o u^- - hu}{ch_o - h},$$

$$(48) \quad \frac{ch_o u^- - hu}{ch_o - h} = \frac{ch_o (u^-)^2 - hu^2 - p}{ch_o u^- - hu},$$

$$(49) \quad s^+ = \frac{cu^+ - u}{c - 1},$$

$$(50) \quad \frac{cu^+ - u}{c - 1} = \frac{ch_o u^+ - hu}{ch_o - h},$$

$$(51) \quad \frac{ch_o u^+ - hu}{ch_o - h} = \frac{ch_o (u^+)^2 - hu^2 - p}{ch_o u^+ - hu}.$$

Having six equations to constrain five unknowns ( $s^-$ ,  $s^+$ ,  $u$ ,  $p$ , and  $h$ ) opens the possibility for inconsistency. However, as we will see below, (47) and (50) are, in fact, redundant.

Solving (48) and (51) for  $p$  yields

$$(52) \quad p = \frac{ch_o h (u^- - u)^2}{h - ch_o}$$

and

$$(53) \quad p = \frac{ch_o h (u^+ - u)^2}{h - ch_o}.$$

By assumption,  $c \neq 0$ . One can also assume that  $h \neq 0$  and  $h_o \neq 0$ , since this would mean that there is no ice near this interface and  $u$  becomes arbitrarily defined. Hence,

$$(54) \quad (u^- - u)^2 = (u^+ - u)^2.$$

Also,  $u^- > u^+$  in the convergence case considered here, so that

$$(55) \quad u^- - u = u - u^+.$$

It follows that

$$(56) \quad u = \frac{u^- + u^+}{2}.$$

Note that one may have predicted this result, namely that the ice masses, once consolidated, move at the average velocity (since ice thickness and concentration are equal on each side).

Using (47), one can solve for  $h$ —which, as one might expect, turns out to be equal to  $h_o$ . (Since a finite ice strength does not enter this picture, there should not be any yielding or change in thickness.) Equation (50) yields the same answer (showing that one of them is unnecessary).

Substituting expression (56) for  $u$  into (46) and (49), we can solve for the two shock speeds:

$$(57) \quad s^- = \frac{u^+ + u^-(1 - 2c)}{2(1 - c)}, \quad s^+ = \frac{u^- + u^+(1 - 2c)}{2(1 - c)}.$$

In order for the picture in Figure 10 to be accurate, we also need that  $s^- < s^+$ . This is true.

*Proof.* Since we are only concerned with convergence,  $u^- > u^+$ . From (56), it can be concluded that  $u^- > u > u^+$ . Also  $0 < c < 1$ . It follows that

$$(58) \quad cu^- > cu, \quad cu > cu^+,$$

$$(59) \quad u - cu^- < u - cu, \quad u - cu < u - cu^+,$$

$$(60) \quad \frac{u - cu^-}{1 - c} < u, \quad u < \frac{u - cu^+}{1 - c},$$

$$(61) \quad s^- < u, \quad u < s^+,$$

where (46) and (49) were used for the last step.  $\square$

The interpolation scheme resulting from this analysis is the following:

$$(62) \quad u_{j+\frac{1}{2}} = \begin{cases} u^- & \text{if } u^- \geq u^+, 0 < s^- < s^+, \\ u^+ & \text{if } u^- \geq u^+, s^- < s^+ < 0, \\ u = \frac{u^- + u^+}{2} & \text{if } u^- \geq u^+, s^- \leq 0 \leq s^+. \end{cases}$$

(We have chosen to group the cases  $s^- = 0$  and  $s^+ = 0$  into the last category, while they could as well fit into the two previous scenarios, respectively.)

Finally, we will say a word about the cases  $c = 0$  and  $c = 1$ . If  $c = 0$ , there is no ice near the interface, and the velocity of the nonexisting ice is arbitrary. For consistency and smoothness, we will continue to use the same interpolation scheme as above (even though the derivation does not necessarily hold, starting with the observation that the concentration needs to be 1 between the shocks).

If  $c = 1$ , the ice is consolidated around the interface in question, which means that it should all be traveling at the same speed (in the absence of crushing). In other words,  $u^- = u^+$ . If this is not the case, due to numerical error, we set

$$(63) \quad u_{j+\frac{1}{2}} = \frac{u^- + u^+}{2}.$$

This completes the description of the interpolation scheme.

**Acknowledgment.** We would like to thank David Holland for his comments on this work.

#### REFERENCES

- [1] M.C. COON, *Mechanical behavior of compacted arctic ice floes*, J. Pet. Technol., 26 (1974), pp. 466–470.
- [2] M.C. COON, S.A. MAYKUT, R.S. PRITCHARD, D.A. ROTHROCK, AND A.S. THORNDIKE, *Modeling the pack ice as an elastic-plastic material*, AIDJEX Bull., 24 (1974), pp. 1–105.
- [3] G.M. FLATO AND W.D. HIBLER, III, *Modeling pack ice as a cavitating fluid*, J. Phys. Oceanogr., 22 (1992), pp. 626–651.
- [4] W.D. HIBLER, III, *A dynamic thermodynamic sea ice model*, J. Phys. Oceanogr., 9 (1979), pp. 817–846.
- [5] E.C. HUNKE AND J.K. DUKOWICZ, *An elastic-viscous-plastic model for sea ice dynamics*, J. Phys. Oceanogr., 27 (1997), pp. 1849–1867.
- [6] H.S. HUNTLEY, E.H. SUH, AND E.G. TABAK, *An optimization approach to modeling sea ice dynamics. Part 1: Lagrangian framework*, SIAM J. Appl. Math., to appear.
- [7] R.J. LEVEQUE, *Numerical Methods for Conservation Laws*, 2nd ed., Birkhäuser Boston, Cambridge, MA, 1992.

- [8] J.E. OVERLAND AND C.H. PEASE, *Modeling ice dynamics of coastal seas*, J. Geophys. Res., 93 (1988), pp. 15619–15637.
- [9] R.S. PRITCHARD, *An elastic-plastic constitutive law for sea ice*, J. Appl. Mech., 42E (1975), pp. 379–384.
- [10] H. SCHAFFRIN, *An Optimization Approach to Sea Ice Dynamics*, Ph.D. thesis, Department of Mathematics, Courant Institute of Mathematical Sciences, New York University, New York, NY, 2005.
- [11] A.S. THORNDIKE, D.A. ROTHROCK, G.A. MAYKUT, AND R. COLONY, *The thickness distribution of sea ice*, J. Geophys. Res., 80 (1975), pp. 4501–4513.
- [12] L.-B. TREMBLAY AND L.A. MYSAK, *Modeling sea ice as a granular material, including the dilatancy effect*, J. Phys. Oceanogr., 27 (1997), pp. 2342–2360.